We present field, petrographic, mineral chemical and whole-rock geochemical characteristics of the Neoarchean Verbaard granitoid from the type locality in the central part of the Limpopo Complex in southern Africa. Considering the occurrence of garnet, comparison with garnet-bearing migmatitic metapelite and associated garnet-bearing leucosome from the study area was carried out. Phase equilibria modeling of the migmatitic metapelite and Verbaard granitoid compositions is used to reconstruct P-T conditions of their evolution. After evaluating the provenance of garnet associated with the Verbaard granitoid, petrogenetic characterization of carefully selected granitoid samples was attempted. The results are compared with the data on other related Neoarchean granitoids from the region.

2. Geologic setting

The region between the southern margin of the Archean Zimbabwe Craton and the northeastern margin of the Archean Kaapvaal Craton constitute the Limpopo Complex high-grade (amphibolite- to granulite-facies metamorphic) terrane (Fig. 1a, b). The central portion of this Paleoarchean to Paleoproterozoic terrane is referred to as the Central Zone, while those along the respective cratonic margins are the Northern Marginal Zone and the Southern Marginal Zone (Fig. 1b). Kilometer-scale shear zones separate the different zones from one another and also from the adjacent cratons (see reviews in Blenkinsop, 2011; Smit et al., 2011; Van Reenen et al., 2011).

The Central Zone includes the Beit Bridge Complex, Phikwe Complex and the Mahalapye Complex terranes (Fig. 1b; Aldiss, 1991). The rocks described in this paper are from the Beit Bridge Complex, the largest of the Central Zone terranes. Like a typical high-grade terrane, voluminous granitoids and less dominant deformed supracrustal rocks make up the Beit Bridge Complex. Sedimentary rocks deposited before ~3.3 Ga of the Beit Bridge Group constitute the oldest unit. These rocks together with minor mafic to ultramafic rocks of the ~3.35 Ga Messina layered intrusion occur interleaved within voluminous granitoids (e.g., Fig. 1c). The prominent granitoid events include the ~3.31–3.28 Ga migmatitic Sand River tonalite-trondhjemite-granodiorite gneiss and

Fig. 1. (a) TM742 compilation of southern Africa showing the approximate extent of the Archean Kaapvaal and Zimbabwe cratons. The box indicates the area covered in (b). (b) Generalized geologic map of the Limpopo Complex showing the approximate extents of the three zones, Southern Marginal Zone, Central Zone and Northern Marginal Zone, with respect to the adjacent cratons. Approximate extents of the different complexes – Beit Bridge Complex, Phikwe Complex, Mahalapye Complex and Motloutse Complex – are also shown [modified from Aldiss, 1991]. The box indicates the area covered in (c). sz – shear zone. Dsz – Dikalate shear zone; Msz – Magogaphate shear zone. (c) Geologic map of the Musina area showing the study area [modified after Rajesh et al., 2018a]. Tsz - Tshipise shear zone. (d) Satellite image showing the extent of the study area including the mapped section (referred as the Verbaard area) and the O6–19 outcrop (S 22°26′11.4″, E 30°00′33.7″) to the northeast of the Verbaard farm, and covers the area indicated by the rectangle in (c). (e) Geological map of the mapped section indicated in (d) showing the occurrence of Verbaard granitoid and its relation to other rock types.

various ~2.73–2.58 Ga granitoids (Alldays, Singelele, Avoca, and Bulai granitoids) (see reviews in Smit et al., 2011; Kramers et al., 2011). Two high-grade tectono-metamorphic events have been prominently documented from the Beit Bridge Complex. The earlier ~2.72 to 2.61 Ga event is correlated with the intrusion of voluminous granitoids, while the ~2.04 to 2.01 Ga event is manifested by minor anatectic intrusions, granitic pegmatites, reactivation along faults/shear zones and metasomatic overprint (Brandt et al., 2018; Gerdes and Zeh, 2009; Holzer et al., 1998; Jaeckel et al., 1997; Kröner et al., 1999, 2018; Mouri et al., 2009; Van Reenen et al., 2004, 2008; Zeh et al., 2007, 2010).

The present study is focused on the Verbaard granitoid, which belongs to the group of the Neoarchean granitoids within the Beit Bridge Complex. The studied localities are situated southwest of Musina along the river pavements of the Sand River (Fig. 1c).

3. Field relations

Two varieties of the Verbaard granitoid – tonalitic and granodioritic – have been reported (Jaeckel et al., 1997; Hofmaan et al., 1998). The light-grey granodioritic variety forms dyke-like continuous layers within the dark-grey tonalitic variety and displays intrusive marginal apophyses in the dark-grey rock. These relations indicate that the emplacement of the tonalitic variety predates the intrusion of the granodioritic variety (cf. Hofmaan et al., 1998). This is supported by Pb—Pb zircon ages of 2647 ± 0.4 Ma and 2615.6 ± 0.2 Ma from the tonalitic and granodioritic Verbaard rock types, respectively (Jaeckel et al., 1997). Kröner et al. (1999) further reported a Pb—Pb zircon age of 2629 ± 3 Ma from the granodioritic variety. The dark-grey tonalites contain abundant centimetre- to decimetre-scale enclaves of the Sand River granitoid gneisses and amphibolites. The light-grey granodiorites are characterized by a spectacular network of leucocratic veins.

The study area covers the mapped section within the Verbaard farm (referred here as the Verbaard area) and the O6–19 outcrop [the notation O6–19 follows the usage by previous studies (Boshoff, 2008; Perchuk et al., 2008; Van Reenen et al., 2008)] to the northeast of the Verbaard area (Fig. 1d). The Verbaard area (Fig. 1e) can be divided into four groups. The oldest group including metaquartzite, metapelite and meta-ironstone belongs to the Beit Bridge Group supracrustals. Ultramafic (peridotite, pyroxenite) and mafic (gabbro) rocks are part of the Paleoarchean Messina layered intrusion. Three types of granitoids – the Neoarchean Verbaard granitoid, the Neoarchean Singelele leucogranite and the Paleoproterozoic leucogranite – occur in the study area. Dolerite dyke is the youngest rock in the study area. The present paper describes metapelite, associated leucosome, and the Verbaard granitoid. Nearby rocks which exhibit the occurrence of garnet and/or anatectic overprint are also mentioned.

Two types of migmatitic metapelites occur in the study area. They correspond to the two types (high-Al and low-Al) of metapelites recognized based on bulk-rock chemical alumina content by Boryta and Condie (1990) from the Musina area. The darker coloured high-Al migmatitic metapelite (Fig. 2a) is mostly composed of residual material, garnet-biotite-sillimanite-cordierite. In contrast, the lighter coloured low-Al migmatitic metapelite (Fig. 2b) contains higher proportions of leucocratic material. The one exposed at the O6–19 outcrop is a high-Al migmatitic metapelite (Figs. 1d, 2c). Biotite-rich melanocratic layers delineate the margins of leucosomes. In general, the size of garnet increases from the restitic domains to the irregular outline leucosomes, often forming aggregates in the latter. Leucosomes associated with metapelite at the O6–19 outcrop hosts some of the largest garnet crystals (Fig. 2c). The leucosomes, considered to be product of partial melting, are generally concordant to the gneissic fabric (Fig. 2a, b). Locally, they cross cut the gneissic fabric (Fig. 2c). With segregation of melt, boudinaging and intrafolial folds develop within the rock.

Garnet occurs locally within the meta-ironstone and gabbro. Leucocratic veins locally intrude the gabbroic bodies (Fig. 2d). No garnet or leucocratic veins occur in the ultramafic rocks.

Among Neoarchean granitoids in the Verbaard area, the Verbaard granitoid constitutes the dominant type, whereas the Singelele leucogranite is less common. Unlike the Verbaard granitoid, garnet is uniformly distributed as part of the primary magmatic assemblage in the Singelele leucogranite. No anatectic overprint occurs in the Singelele leucogranite.

The biotite-bearing Verbaard granitoid is represented by a number of light-grey homogeneous bodies intruding into the metapelite (Figs. 1e, 2e). Weathered surfaces are pinkish to brownish. The weak biotite-defined foliation in the granitoid is generally parallel to the gneissic fabric of the metapelite (Fig. 2f). No enclaves of surrounding rock were found in the granitoid bodies. The Verbaard granitoid bodies show a network of garnet-bearing leucocratic veins (Fig. 2f to h). They are dominantly concordant to the gneissic foliation (Fig. 2f to h). Unlike the leucosomes in the migmatitic metapelite, the leucocratic veins in the Verbaard granitoid are characterized by more or less straight line margins and are not outlined by any biotite-rich melanocratic margins. The garnet grains often aggregate towards the center of these anatectic leucocratic veins (Fig. 2h). Sampling of Verbaard granitoid for the present study was carried out from exposures like the ones illustrated in Fig. 2e to h.

4. Petrography

Both high-Al and low-Al migmatitic metapelite have more or less similar mineralogy, but differ on microstructure. The high-Al rock is characterized by melanocratic biotite-sillimanite-cordierite layers of variable thickness (~0.01–0.04 mm) separated by thin (<0.3 mm) quartzofeldspathic layers (Fig. 3a). Cordierite is altered to pinite and sericite (Fig. 3a), giving the yellow-brown colour to the melanocratic layers. Prismatic and fibrous crystals of sillimanite are prominently concentrated in the central portions, while biotite occurs in the central and marginal portions (Fig. 3a, b). In comparison, the yellow-brown aluminous layers in the low-Al migmatitic metapelite are thinner (<0.05 mm) and are almost devoid of biotite (Fig. 3c). If present, biotite dominantly occurs along the margins of layers. The felsic minerals have lobate rounded grain margins. Both migmatitic metapelites indicate a transition in the mode of occurrence of quartz and feldspar from more or less patchy occurrence (Fig. 3d) to thin elongated grains (Fig. 3e) to larger grains generally elongated parallel to the length of the aluminous layers (Fig. 3f). Due to higher melt content, the low-Al rock is richer in quartzofeldspathic material than the high-Al one.

Garnet is locally associated with the aluminous layers in both migmatitic metapelites (Fig. 3g to j). It is always surrounded by cordierite, sillimanite and biotite (Fig. 3g to j). The occurrence of garnet in the quartzofeldspathic layers varies from small grains to large porphyroblasts; the larger ones occur at the leucocratic portions. They can have straight line as well as lobate rounded grain margins. Garnet contains rare inclusions of quartz, biotite and sillimanite. Quartz and feldspar grains towards the leucocratic portions are characterized by medium- to coarse-grain size and lobate rounded grain margins (Fig. 3k to n). Perthite and myrmekite occur locally (Fig. 3k). Unlike the metapelite, the associated leucosomes are dominated by coarse-grained plagioclase and quartz (Fig. 3o, p). Plagioclase is sericitized and quartz often shows undulatory extinction. Subhedral plagioclase can be densely packed with the crystals touching at the corners or along crystal faces to form a framework and indicative of compaction (see inset in Fig. 3o; e.g., Carvalho et al., 2016). Large garnet crystals occur either as rounded grains or irregular aggregates, both exhibiting lobate rounded grain margins (Fig. 3p).

The Verbaard granitoid is dominantly made up of plagioclase, K-feldspar and quartz (Fig. 3q to s). Albite twins in plagioclase and undulatory extinction of quartz are common. Biotite is the dominant mafic mineral, occurring interstitial to the felsic minerals. Minor Fe—Ti oxides occur. In some samples, biotite defines a feebly visible gneissic fabric. Elongated quartz and feldspar further enhance the gneissic fabric. Felsic minerals

Fig. 2. Field photographs from the Verbaard area illustrating the occurrence of the two types of migmatitic metapelite – darker high-Al (a) and lighter low-Al (b), migmatitic metapelite with associated garnet-bearing leucosome at the O6–19 outcrop (c), leucocratic veins intruding the gabbro (d), intrusive relation of the Verbaard granitoid with the metapelite (e), and the conspicuous garnet-bearing leucocratic veins associated with the Verbaard granitoid (f to h).

contain inclusions of biotite (Fig. 3s). Perthite and myrmekite occurs locally (Fig. 3t). Two types of grain margins occur – straight line and lobate rounded. The straight line grain margins are prominently associated with the primary magmatic texture. On the other hand, the curved lobate grain margins which often protrude along the length of straight grains indicate that they are late with respect to the earlier straight grain margins. They are likely related to the anatectic overprint.

Garnet occurs in two modes in the Verbaard granitoid. In addition to large porphyroblasts in leucocratic veins (Fig. 3w), small grains of garnet are present in the matrix of the Verbaard granitoid (Fig. 3u, v). The latter was found only in few of the studied Verbaard granitoid samples. Inclusions in garnet are represented by quartz and minor biotite. In comparison to the medium-grained felsic minerals in the Verbaard granitoid, quartz and feldspars in the leucocratic veins are coarse-grained (Fig. 3x). K-feldspar is the dominant feldspar in the leucocratic vein (Fig. 3x).

5. Analytical methods

Major element contents of minerals in polished thin sections were obtained using an electron microprobe (CAMECA SX100) equipped with four wavelength dispersive spectrometers housed at the University of Johannesburg. The analyses were obtained using an accelerating voltage of 15 kV, beam current of 20 nA, beam size of 1–5 μm and counting time of 10–20 s. The ZAF correction procedure was applied to the data.

Major and some trace elements of representative samples were determined on fused lithium tetraborate (sample to flux ratio of 1:10) glass beads using standard XRF techniques at ACME Labs, Canada. Loss on ignition (LOI) by mass was calculated by the weight difference after ignition to 1000 °C. Additional trace and rare earth elements (REE) have been analyzed by inductively coupled plasma mass spectrometry, following a lithium metaborate/tetraborate fusion and nitric acid digestion, also at ACME Labs. Accuracy has been controlled by replicate analysis against international rock standards and the results are in good agreement with the recommended values – 2–5% (1σ) for most elements and $\pm$ 10% for U, Nd, and Ni.

6. Mineral chemistry

The mineral composition is given as Supplementary online material Tables DR1 to 5. Mineral abbreviations are after Whitney and Evans (2010).

Garnet in both high-Al and low-Al migmatitic metapelites is pyrope-almandine, with minor grossular and spessartine components: $Prp_{23-32}Alm_{63-73}$ in high-Al migmatitic metapelite and $Prp_{27-30}Alm_{66-69}$ in low-Al migmatitic metapelite (Fig. 4a, b; Table DR1). The grossular content is lower in the low-Al (1.5–2.4 mol%) rock than the high-Al (2–3.5 mol%) one.

Garnet in the Verbaard granitoid and leucocratic veins have similar compositions: $Prp_{28-29}Alm_{65-67}$ in the Verbaard granitoid and $Prp_{27-29}Alm_{65-67}$ in the leucocratic vein (Fig. 4a, b; Table DR2). They differ slightly in the grossular content. Garnet in the leucocratic veins contains 1 to 4 mol% of grossular, while garnet in the Verbaard granitoid contains 1 to 2 mol% of grossular.

The largest garnets preserved in the leucosomes associated with the high-Al migmatitic metapelite (O6-19) are also pyrope-almandine with minor grossular and spessartine components (Fig. 4a, b; Table DR3). But, the individual contents are slightly different from those in the metapelite and Verbaard granitoid. Pyrope and grossular contents respectively range from 30 to 38 mol% and 2 to 8 mol% (Table DR3), and are the largest among the different rocks. On the other hand, almandine content is the lowest among the different rocks, ranging from 56 to 60 mol%.

Fig. 5 shows rim-core-rim chemical profiles for garnets in the Verbaard granitoid, leucocratic vein associated with the Verbaard granitoid, low-Al migmatitic metapelite and leucosome associated with the high-Al migmatitic metapelite (O6-19). Garnets from the low-Al migmatitic metapelite and the Verbaard granitoid show very slight or no zoning for X_{Mg} [$= Mg/(Mg + Fe^{2+} + Mn) = 0.28-0.31$ in low-Al migmatitic metapelite and 0.29–0.30 in Verbaard granitoid] and X_{Ca} [$= Ca/(Ca + Mg + Fe^{2+} + Mn) = 0.02$ in low-Al migmatitic metapelite and 0.03–0.04 in Verbaard granitoid] (Fig. 5a, c). In contrast, large garnet from leucosome associated with the high-Al migmatitic metapelite (O6-19) shows an increase of X_{Mg}^{Grt} from 0.32 in core to 0.36 in both rims, whereas X_{Ca}^{Grt}, being constant throughout most of the grain, abruptly decreases in rims from 0.08 to 0.03 (Fig. 5b). Similar decrease of X_{Ca} (from 0.06 to 0.03) at constant X_{Mg} (0.29-0.30) is observed also for large garnet from leucocratic vein associated with the Verbaard granitoid (Fig. 5d).

Biotite in the high-Al migmatitic metapelite shows X_{Mg} ($= Mg/(Mg + Fe)$) = 0.52–0.57, and 0.53 to 0.74 apfu (atoms per formula unit) Ti, 2.90 to 3.02 apfu Al, and 1.73 to 1.83 apfu K (Fig. 4c, d; Table DR4a). Biotite in the low-Al migmatitic metapelite has a higher X_{Mg} (0.54–0.68) and Al content (2.85–3.17 apfu), and lower Ti (0.18–0.56 apfu) and K (1.28–1.73 apfu) contents (Fig. 4c, d; Table DR4b). Biotite in the Verbaard granitoid shows X_{Mg} = 0.48–0.50, and 0.71 to 0.81 apfu Ti, 2.81 to 3.06 apfu Al, and 1.76 to 1.85 apfu K (Fig. 4c, d; Table DR4c). In comparison to the migmatitic metapelites, biotite in the Verbaard granitoid has lower X_{Mg} (Fig. 4c, d).

Anorthite [An ($= Ca/Ca + Na + K$)] contents of plagioclase in the Verbaard granitoid (An_{22}-An_{25}) and in the migmatitic metapelites (An_{21}-An_{24}) are relatively similar (Table DR5). The K-feldspar composition in the migmatitic metapelites is in the range of Or_{83} to Or_{93}, while that of the Verbaard granitoid reaches higher orthoclase content (Or_{93-97}) (Table DR5).

7. Whole-rock geochemistry

Each of the rock samples was carefully selected for bulk geochemical analysis, after making sure of least contamination (through petrographic examination of thin section from the same sample). The

Fig. 3. Representative photomicrographs and BSE images illustrating the mineralogic and textural features of migmatitic metapelites, associated leucosomes, the Verbaard granitoid and associated leucocratic veins. (a, b) the conspicuous thicker cordierite-biotite-sillimanite-dominant yellow-brown layers in the high-Al migmatitic metapelite, (c) thinner and less prominent cordierite-sillimanite-dominant yellow-brown layers in the low-Al migmatitic metapelite, (d to f) mode of occurrence of quartz and feldspar indicate a transition from more or less patchy occurrence (d) to thin elongated grains (e) to larger grains generally elongated parallel to the length of the aluminous layers (f). (g to j) the mode of occurrence of garnet associated with the aluminous layers/patches in the high-Al (g, i) and low-Al migmatitic metapelite (h, j), (k) the local occurrence of perthitic K-feldspar and myrmekite in the migmatitic metapelite, (l to n) the transition from medium-grained to coarse-grained quartzofeldspathic material observed towards the leucocratic portion, and, (o, p) the coarse-grained minerals including plagioclase (o) and garnet [only a portion shown in (p)] in leucosomesassociated with the migmatitic metapelites. The inset in (o) shows portion of a region where subhedral plagioclase is densely packed with the crystals touching at the corners or along crystal faces to form a framework. (q to s) the mode of occurrence of plagioclase, quartz, K-feldspar and biotite in the Verbaard granitoid, (t) the local occurrence of perthite and myrmekite in the Verbaard granitoid, (u, v) the garnet grains occurring locally within the Verbaard granitoid, and (w, x) the coarse-grained quartzofeldspathic minerals and garnet in leucocratic veins associated with the Verbaard granitoid. Crd – cordierite; Sil – sillimanite; Bt – biotite; Qz – quartz; Kfs – K-feldspar; Pl – plagioclase; Grt – garnet; Per – perthite; Myr – myrmekite; Zr – zircon; (a to h), (u), (w) – photomicrographs taken under PPL; (k to o), (q to t), (x) – photomicrographs taken under XPL; (i), (j), (p), (v) – BSE images.

Fig. 3 (*continued*).

Fig. 3 (*continued*).

Fig. 4. Mineral chemistry based diagrams illustrating the variation of garnet and biotite compositions from migmatitic metapelites, associated leucosome, the Verbaard granitoid and associated leucocratic vein. (a) X_{Ca} versus X_{Mg} of garnet, (b) X_{Mn} [= $Mn/(Mg + Fe^{2+} + Mn)$] versus X_{Mg} of garnet, (c) Ti (apfu) versus X_{Mg} of biotite, and (d) Al_t (apfu) versus X_{Mg} of biotite; t – total.

Fig. 5. Representative rim-core-rim garnet mineral chemcial profiles in terms of X_{Mg} and X_{Ca} from the low-Al migmatitic metapelite (a), leucosome associated with high-Al migmatitic metapelite at O6–19 (b), Verbaard granitoid (c), and leucocratic vein associated with the Verbaard granitoid (d). X_{Mg} (red points) is indicated on the left axis, while X_{Ca} (green points) is indicated on the right axis in all the digrams. The corresponding data set are given in Tables DR1 to 3. Closer to minor chlorite inclusions, garnet becomes slightly Fe-rich and accounts for two of the minor troughs observed between ~4 and 12 mm distance in (b).

greatest challenge faced was to sample the biotite-bearing Verbaard granitoid sensu stricto with no garnet or leucocratic vein. A contaminated Verbaard granitoid (with visible garnet-bearing leucocratic vein and minor metapelitic material) was sampled close to the contact with the metapelite, and was also included for geochemical analyses to understand the effect of contamination. Major, trace and rare-earth element data obtained for all the rock samples are given in Tables 1 and 2. For comparison, available data on high-Al and low-Al metapelites from the Musina area by Boryta and Condie (1990) (see Table DR6), the tonalitic and granodioritic Verbaard granitoid samples dated by Jaeckel et al. (1997) (see Table DR6), the granitic Verbaard granitoid sample with associated leucocratic vein dated by Kröner et al. (1999) (see Table DR6) and other related Neoarchean granitoids from the Beit

Bridge Complex [from Rajesh et al., 2018a and references therein] are shown in the different geochemistry-based plots.

7.1. Major element characteristics

The high-Al migmatitic metapelite (sample O6-19M from the O6-19 outcrop) shows lower SiO_2, Na_2O and K_2O contents, and higher total Fe + MgO + TiO_2, Al_2O_3 and CaO than the low-Al migmatitic metapelite (sample MT10) (Fig. 6; Table 1). The major element characteristics of O6-19M and MT10 are respectively comparable to that of high-Al and low-Al metapelites reported by Boryta and Condie (1990) from the Musina area (Fig. 6). Leucosomes associated with both high-Al and low-Al migmatitic metapelites are tonalitic (Fig. 7a), mildly

Table 1
Representative major and trace element data for rocks from the study area.

Sample No	VG8a	VG8b	VG8c	VG8d	VG8e	VG8fg	VGL8f	VGL8h	O6-19L	O6-19M	MT10
Rock type	Verbaard	Verbaard	Verbaard	Verbaard	Verbaard	Verbaard granitoid	leucosome low-Al	leucosome low-Al	leucosome high-Al	High-Al	Low-Al
	granitoid	granitoid	granitoid	granitoid	granitoid	(contaminated)	migm metapelite	migm metapelite	migm metapelite	migm metapelite	migm metapelite
SiO_2	72.77	72.32	72.41	71.30	72.89	71.56	73.83	74.99	72.83	54.09	73.19
TiO_2	0.30	0.30	0.28	0.29	0.31	0.41	0.08	0.06	0.02	1.44	0.31
Al_2O_3	14.89	15.02	14.96	14.58	14.74	15.17	14.79	14.84	16.06	22.48	11.90
Fe_2O_3*	1.57	1.64	1.68	2.10	1.61	3.18	1.13	0.48	0.26	8.03	3.68
MnO	0.01	0.01	0.01	0.01	0.01	0.03	0.03			0.07	0.03
MgO	0.47	0.52	0.52	0.53	0.54	1.86	0.29	0.15	0.03	5.04	2.12
CaO	2.32	2.33	2.30	2.08	2.26	1.32	3.65	4.12	4.13	0.75	0.35
Na_2O	4.18	3.79	3.86	3.49	3.89	2.64	3.77	3.57	4.06	0.46	0.66
K_2O	2.57	3.23	3.09	3.19	2.91	2.24	0.76	0.66	0.88	4.26	5.72
P_2O_5	0.05	0.06	0.06	0.08	0.05	0.02	0.02	0.02	0.03	0.01	0.04
LOI	0.70	0.60	0.70	1.30	0.60	1.30	0.80	0.60	0.85	1.90	0.85
Total	99.83	99.82	99.87	98.95	99.81	99.73	99.15	99.49	99.15	98.53	98.85
ASI	1.08	1.08	1.08	1.13	1.08	1.66	1.08	1.06	1.06	3.34	1.51
Na + K-Ca	4.43	4.69	4.65	4.60	4.54	3.56	0.88	0.11	0.81	3.97	6.03
Fe/Fe + Mg	0.77	0.76	0.76	0.80	0.75	0.63	0.80	0.76	0.90	0.61	0.63
K_2O/Na_2O	0.61	0.85	0.80	0.91	0.75	0.85	0.20	0.18	0.22	9.26	8.67
Mg#	38.02	39.38	38.81	34.08	40.73	54.51	34.46	39.03	19.12	56.25	54.14
Fe_t + Mg + Ti	2.34	2.46	2.48	2.92	2.46	5.45	1.50	0.69	0.31	14.51	6.11
Na_2O/K_2O	1.63	1.17	1.25	1.09	1.34	1.18	4.96	5.41	4.61	0.11	0.12
Quartz (Q)**	33.09	32.31	32.60	33.77	33.62	42.09	40.80	42.70	37.04	26.02	43.66
Corundum (C)	1.13	1.20	1.23	1.80	1.20	6.05	1.18	0.81	0.99	15.77	4.08
Orthoclase (Or)	15.19	19.09	18.26	18.85	17.20	13.24	4.49	3.90	5.20	25.18	33.80
Albite(Ab)	35.37	32.07	32.66	29.53	32.92	22.34	31.90	30.21	34.35	3.89	5.58
Anorthite (An)	11.18	11.17	11.02	9.80	10.89	6.42	17.98	20.31	20.29	3.66	1.48
Cr (ppm)	164.2	109.5	95.8	205.3	95.8	478.9	205.3	203.6	68.4	865.4	342.1
Ni	<20	<20	<20	6.4	<20	78	4.5		2	48.9	15.4
Ba	520	693	672	777	664	680	151.1	250.1	158.7	876.2	1359
Ga	21.7	20.3	21	23.5	20	18.9	17.6	18.4	15.7	33.5	14.9
Hf	4.6	4.2	4	6.8	4.7	3.9	6.2	6	6.1	14.3	13.1
Nb	3	2.4	2.6	1.9	2	5.8	3.4	4.1	3.4	16.6	6.7
Rb	51	61.4	59.6	72.5	59.5	56.9	27	18.8	14.6	156.9	140.5
Sr	218.2	225	233	220.7	230.5	116.2	217.2	216.9	166	60.9	79.1
Th	19.3	13.9	14.5	25	25.3	18	7.4	4.5	5	3.5	3
U	1.8	1.6	1.8		1.9	1.2					
V	33	35	32	24.9	29	94	14.7	14	8.6	174.7	46.9
Zr	153.7	151.7	143	165.7	159	126	84.2	66.9	58.8	270	77.5
Y	2.1	2.1	2.5	2.5	2.8	5.5	8.9	1.8	2.8	24.6	7.3
La	36.3	33	36.7	26.9	39.9	45.4	20.8	19.4	24.9	13.4	14.4
Ce	59.5	56.3	63.2	81.8	69.2	84.4	42.1	44.7	46.6	77.3	102.3
Rb/Ba	0.10	0.09	0.09	0.09	0.09	0.08	0.18	0.08	0.09	0.18	0.10
Rb/Sr	0.23	0.27	0.26	0.33	0.26	0.49	0.12	0.09	0.09	2.58	1.78
Sr/Y	103.90	107.14	93.20	88.28	82.32	21.13	24.40	120.50	59.29	2.48	10.84
Nb/Zr	0.02	0.02	0.02	0.01	0.01	0.05	0.04	0.06	0.06	0.06	0.09
Zr/Hf	33.41	36.12	35.75	24.37	33.83	32.31	13.58	11.15	9.64	18.88	5.92

* Total Fe as Fe_2O_3; ASI - Aluminium saturation index; Na + K-Ca - Na_2O + K_2O-CaO; Fe/Fe + Mg - total Fe/total Fe + MgO; Fe + Mg + Ti - total Fe + MgO + TiO_2.
** CIPW norm; migm – migmatitic.

Table 2
Representative REE data of Verbaard granitoid from the study area.

Sample No	VG8a	VG8b	VG8c	VG8e	VG8fg
Rock type	Verbaard granitoid	Verbaard granitoid	Verbaard granitoid	Verbaard granitoid	Verbaard granitoid (with grt)
La (ppm)	36.3	33	36.7	39.9	45.4
Ce	59.5	56.3	63.2	69.2	84.4
Pr	5.64	5.32	5.91	6.7	8.14
Nd	17.7	16.8	16.9	21.7	27
Sm	2.52	2.22	2.47	3.16	4.29
Eu	0.75	0.74	0.8	0.74	1.15
Gd	1.54	1.46	1.54	2.03	3.26
Tb	0.14	0.14	0.15	0.17	0.35
Dy	0.6	0.51	0.6	0.68	1.49
Ho	0.08	0.06	0.09	0.08	0.2
Er	0.19	0.23	0.25	0.25	0.49
Tm	0.02	0.02	0.02	0.02	0.06
Yb	0.22	0.19	0.25	0.21	0.42
Lu	0.03	0.03	0.03	0.03	0.07
La/Sm$_N$	9.30	9.60	9.59	8.15	6.83
Dy/Yb$_N$	1.83	1.80	1.61	2.17	2.37
Eu/Eu*	1.08	1.18	1.17	0.84	0.90
La/Yb$_N$	118.35	124.58	105.30	136.29	77.54

peraluminous in terms of aluminium saturation index [ASI = molar Al/ (Ca − 1.67P + Na + K = 1.06–1.08] (Shand, 1943) (Fig. 7b), ferroan (high-Al migmatitic metapelite leucosome)/magnesian (low-Al

migmatitic metapelite leucosome) in terms of Fe-number [total Fe/ (total Fe + MgO)] (Fig. 7c) and calcic in terms of the modified alkali index (MALI; Na$_2$O + K$_2$O-CaO) (Fig. 7d).

The selected Verbaard granitoid samples (VG8a to VG8e; no visible garnet or contamination) are granodioritic (Fig. 7a), peraluminous (ASI = 1.08–1.13; Fig. 7b), magnesian (Fig. 7c) and calcic (Fig. 7d). The *contaminated* Verbaard granitoid (Sample VG8fg) with visible garnet bearing leucocratic vein and metapelitic material shows higher total Fe + Mg + Ti, and lower Ca, Na and K contents, than the Verbaard granitoid sensu stricto samples (Fig. 6). The strongly peraluminous (ASI = 1.66) (Fig. 7b) compositions attests to the abundance of garnet in sample VG8fg (Table 1). Kröner et al. (1999) noted that it was difficult to obtain a non-composite sample from the leucocratic vein associated with the Verbaard granitoid. However, the composite Verbaard granitoid+leucocratic vein sample gives an approximate indication of the composition of the leucocratic vein. It is granitic (Fig. 7a), peraluminous (ASI = 1.04; Fig. 7b), ferroan (Fig. 7c) and alkali-calcic (Fig. 7d). As leucocratic veins only occur associated with the granodiorite variety of the Verbaard granitoid, it is inferred that the higher K$_2$O content of the leucocratic vein is responsible for the composite sample to fall in the monzogranite field in Fig. 7a.

7.2. Trace element characteristics

The migmatitic metapelites are characterized by high contents of Cr, Ni, V, Y and Nb. The high-Al migmatitic metapelite has higher contents than the low-Al one (Fig. 8a; Table 1). The felsic rocks have lower Cr, Ni,

Fig. 6. Representative major element Harker diagrams illustrating the bulk compositional characteristics of the migmatitic metapelites, associated leucosomes, and the Verbaard granitoid from the study area. A mixed Verbaard granitoid (sample VG8fg) is included to check for contamination. The composite Verbaard granitoid+leucocratic vein sample is from Kröner et al. (1999). Data on high-Al and low-Al metapelites from the Musina area is from Boryta and Condie (1990).

Fig. 7. The felsic rocks from the study area in terms of in terms of normative An-Ab-Or classification diagram of O'Connor (1965) modified by Barker (1979 (a), aluminium saturation index (ASI) vs SiO₂ plot (b), FeOₜ/(MgO + FeOₜ) vs SiO₂ plot (c), and Na₂O + K₂O-CaO vs SiO₂ plot (d). Data on Alldays and Avoca granitoids are from Rajesh et al. (2018a) and references therein. The tonalitic and granodioritic Verbaard granitoid samples dated by Jaeckel et al. (1997) are included in the different plots. The composite Verbaard granitoid+leucocratic vein sample is from Kröner et al. (1999). The fields in (c) and (d) are from Frost et al. (2001).

V, Y and Nb contents (Fig. 8a; Table 1). The contaminated Verbaard granitoid sample VG8fg has higher Cr, Ni, V, Y and Nb contents than the Verbaard granitoid sensu stricto samples (Table 1).

The Na-rich nature of the felsic rocks is concomitant with high contents of Sr. The Verbaard granitoid has the highest Sr content, followed by leucosomes associated with the migmatitic metapelites (Fig. 8b; Table 1). The contaminated Verbaard granitoid sample VG8fg and migmatitic metapelites have lower Sr contents (Fig. 8b; Table 1). Ba and Rb contents approximately correlate with the K contents of the felsic rocks. The Verbaard granitoid has higher Ba and Rb contents, than the leucosomes associated with migmatitic metapelites (Fig. 8c, d; Table 1). The composite Verbaard granitoid + leucocratic vein sample has higher Ba and Rb contents than the Verbaard granitoid sensu stricto samples (Fig. 8c, d).

In terms of trace element mass ratios, migmatitic metapelites (high-Al migmatitic metapelite: 2.6; low-Al migmatitic metapelite: 1.8) have higher Rb/Sr than the felsic rocks (Verbaard granitoid: 0.23–0.33; leucosomes associated with migmatitic metapelites: 0.09–0.12) (Fig. 8e; Table 1). The contaminated Verbaard granitoid have an Rb/Sr mass ratio of 0.5. In contrast, the Sr/Y mass ratio (Verbaard granitoid: 82-107; leucosomes associated with migmatitic metapelites: 24–121) and Zr/Hf (Verbaard granitoid: 24–36; leucosomes associated with migmatitic metapelites: 10–14) mass ratios are higher in the felsic rocks than the migmatitic metapelites [high-Al migmatitic metapelite: 2.5 (Sr/Y), 19 (Zr/Hf); low-Al migmatitic metapelite: 11 (Sr/Y), 6 (Zr/

Hf)] (Fig. 8e, f; Table 1). The contaminated Verbaard granitoid has a Sr/Y mass ratio of 21 and Zr/Hf mass ratio of 32 (Table 1).

In the primitive-mantle normalized (Sun and McDonough, 1989) multi-element spider gram, the Verbaard granitoid sensu stricto and contaminated Verbaard granitoid sample VG8fg show similar large ion lithophile element (LILE) enrichment, with high-field strength element (HFSE) depleted pattern, and negative Nb, Ta, P and Ti anomalies (Fig. 9a). The chondrite-normalized (Sun and McDonough, 1989) REE patterns of the rocks also show similar pattern with enrichment of light REE (LREE, e.g., La) relative to middle REE (MREE, e.g., Sm) [(La/Sm)ₙ – Verbaard granitoid sensu stricto: 8.2–9.6; contaminated Verbaard granitoid sample VG8fg: 6.8] and depletion of heavy REE (HREE, e.g., Yb) [(Gd/Yb)ₙ – Verbaard granitoid sensu stricto: 1.6–2.2; contaminated Verbaard granitoid sample VG8fg: 2.4] (Fig. 9b; Table 2). Among the Verbaard granitoid sensu stricto samples, those which are plagioclase rich have positive Eu anomalies (Eu/Eu* = 1.08–1.18). The contaminated Verbaard granitoid sample VG8fg has a Eu/Eu* value of 0.9 (Table 2).

8. Discussion

As expressed in leucosomes and leucocratic veins, both migmatitic metapelite and the granodioritic Verbaard granitoid from the study area are overprinted by anatexis. The small garnet grains occurring within the granitoid and those associated with leucocratic veins have

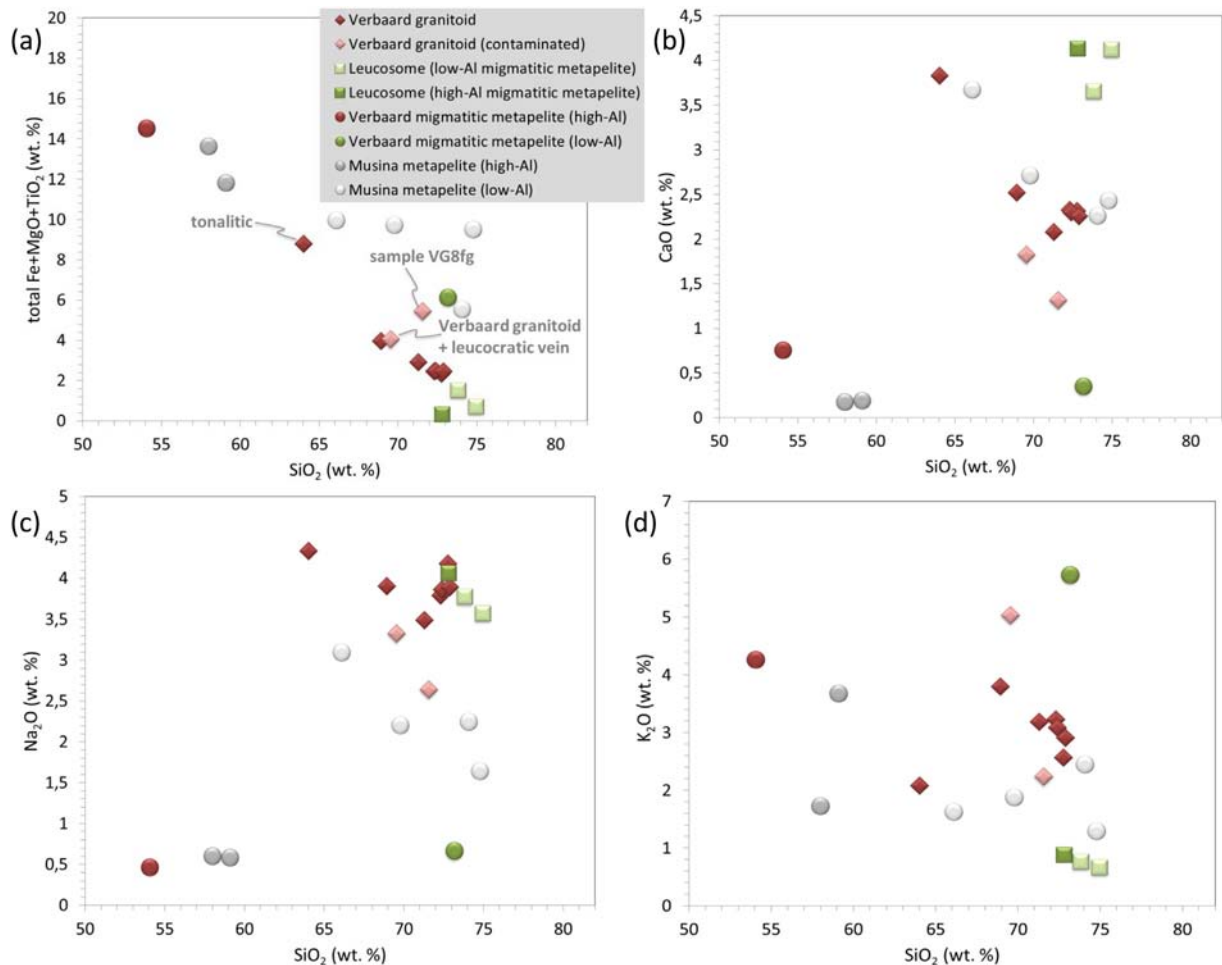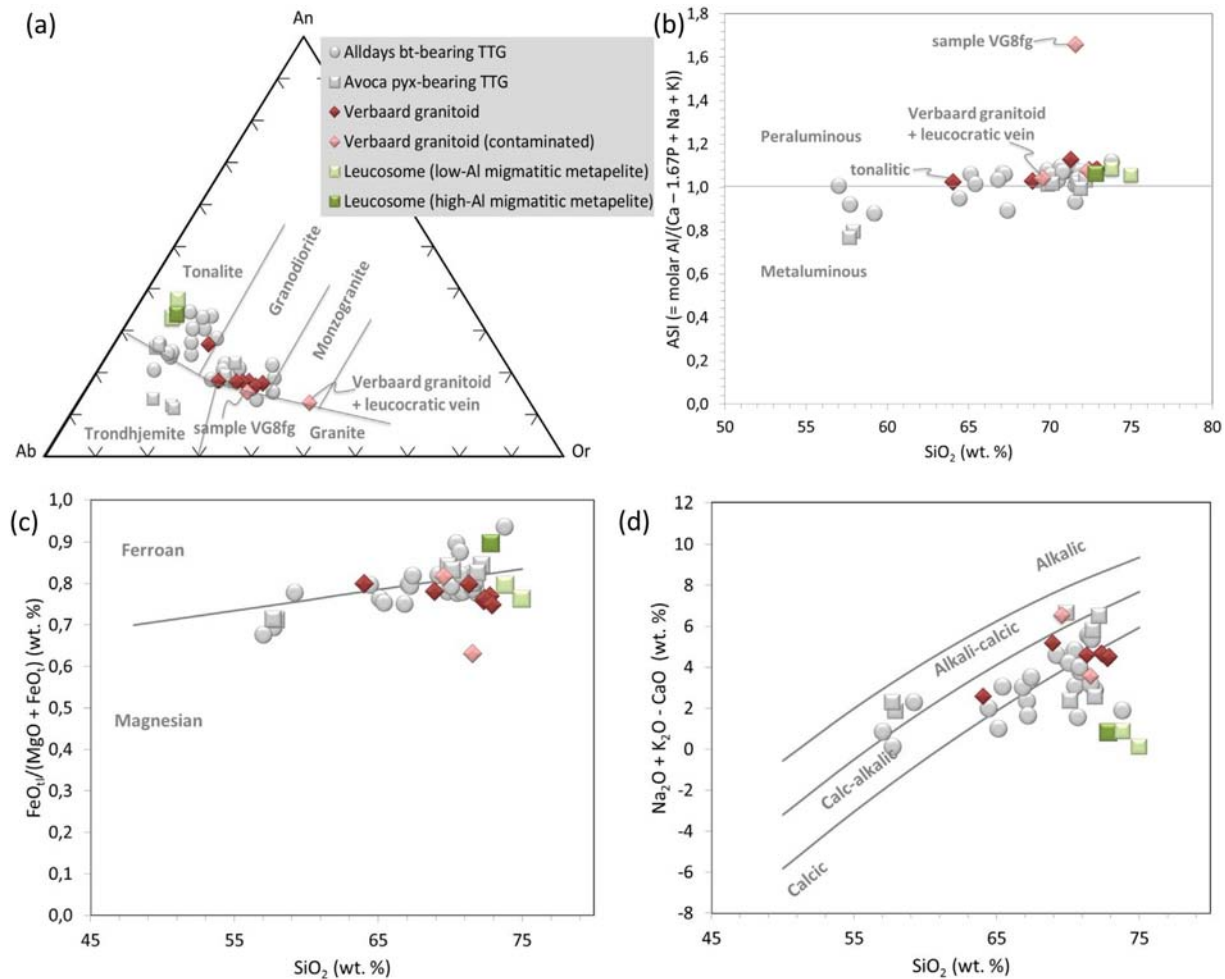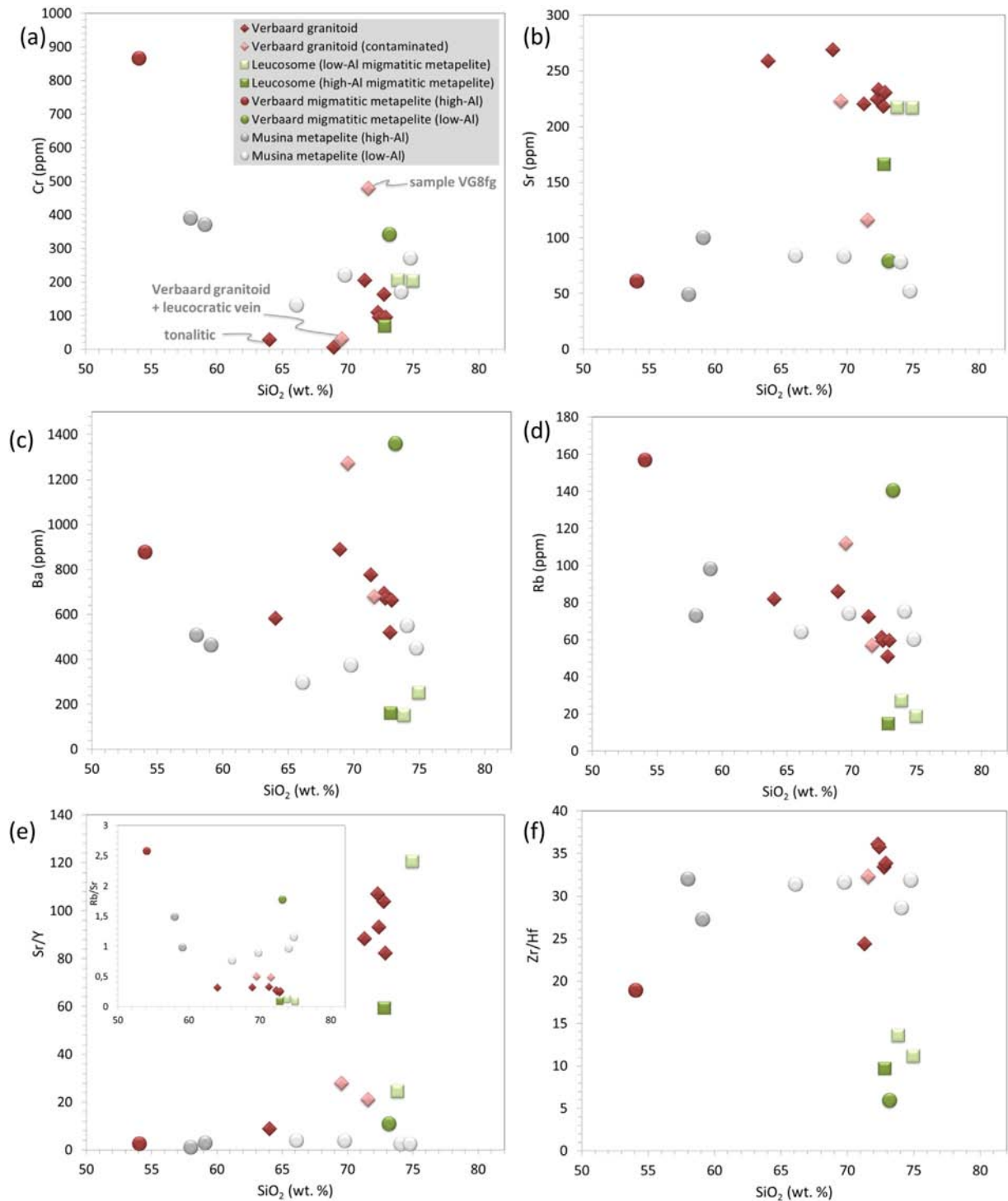**Fig. 8.** Representative trace element (a to d) and trace element mass ratio (e, f) Harker diagrams illustrating the bulk compositional characteristics of the migmatitic metapelites, associated leucosomes, and the Verbaard granitoid from the study area. Like the main diagram, the inset in (e) has SiO₂ (wt%) along the x-axis. A mixed Verbaard granitoid (sample VG8fg) is included to check for contamination. The composite Verbaard granitoid + leucocratic vein sample is from Kröner et al. (1999). Data on high-Al and low-Al metapelites from the Musina area is from Boryta and Condie (1990).

overlapping mineral chemical characteristics (Fig. 4a, b), indicating that both were related to the anatectic event which overprinted the granitoid. Thus, unlike the uniformly distributed biotite, the locally occurring garnet is not part of the primary magmatic assemblage in the Verbaard granitoid. Significantly, garnet compositional characteristics from both migmatitic metapelite/Verbaard granitoid and associated leucosomes/leucocratic veins are comparable. It could imply that both the rocks were subjected to the same overprint event. To evaluate this and

estimate the formation conditions of the garnet-bearing assemblages in both rocks, results of phase equilibria modeling is presented first in this section. After establishing the provenance of garnet found associated with the Verbaard granitoid and understanding its implications, petrogenetic characterization is attempted. Discussion on the phase equilibria modeling results and timing of high-grade events serves the first purpose, while the latter on petrogenesis is done in order to compare to related Neoarchean granitoids from the Beit Bridge Complex terrane.
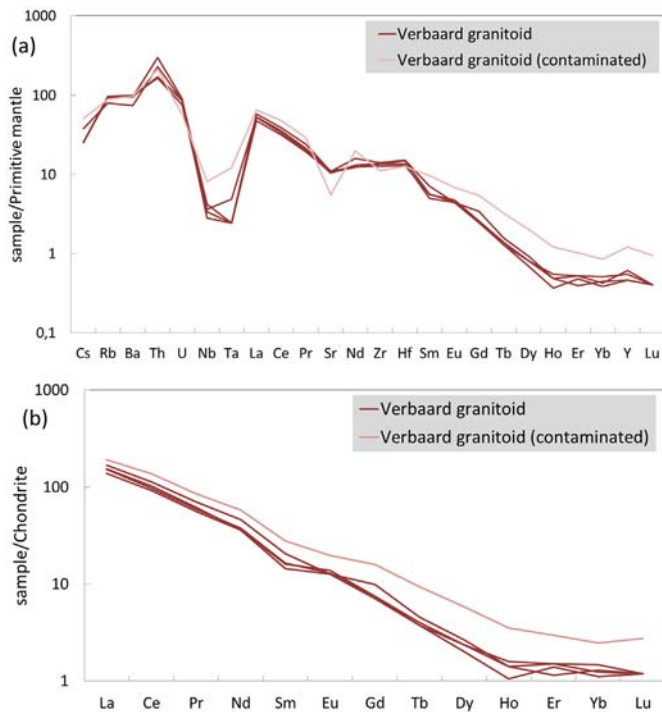
Fig. 9. Primitive mantle-normalized (Sun and McDonough, 1989) trace element spider gram (a) and chondrite-normalized (Sun and McDonough, 1989) REE diagram (b) of the Verbaard granitoid sensu stricto and contaminated Verbaard granitoid (sample VG8fg) from the study area.

8.1. Phase equilibria modeling of high-Al migmatitic metapelite and the Verbaard granitoid

8.1.1. Modeling procedure

Phase equilibria modeling of high-Al migmatitic metapelite (sample O6-19M; Table 1) and the Verbaard granitoid (sample VG8; average of samples VG8a to e in Table 1) was performed via the Gibbs free energy minimization in the system MnO–Na₂O–CaO–K₂O–FeO–MgO–Al₂O₃–SiO₂–H₂O–TiO₂–O₂ (MnNCKFMASHTO) using the PERPLE_X software (Connolly, 2005) version 6.7.7 for Windows. The standard properties database hp11ver.dat (Holland and Powell, 2011) and solution model database solution_model.dat (http://www.perplex.ethz.ch) were applied for modeling. The following models from White et al. (2014) were applied for mineral solutions (see descriptions at http://www.perplex.ethz.ch/perplex/datafiles/solution_model.dat): Gt(W) for Fe^{3+}-bearing Ca-Mg-Fe-Mn garnet, Bi(W) for Ti and Fe^{3+}-bearing biotite and Crd(W) for hydrous cordierite. The model "feldspar" based on the solution model of Fuhrman and Lindsley (1988) was taken for ternary feldspar and model Ilm(WPH) was applied for the ilmenite solid solution (White et al., 2000). The model melt(W) from White et al. (2014) was used for the NCKFMASH silicate melt.

8.1.2. High-Al migmatitic metapelite (O6-19M)

Pseudosection for the high-Al migmatitic metapelite was calculated at the arbitrary "free" O_2 (which serves as a monitor of Fe_2O_3) content 0.01 wt%. This value was taken arbitrarily. Construction of the T-M_{O2} (where M_{O2} is the "free" O_2 content, wt%, in the system) showed that phase relations and, thus, phase compositions are independent of the O_2 content in the system within a wide interval (Fig. DR7), probably, because of high content of biotite, which takes all ferric iron. Water content was estimated using the T-M_{H2O} (where M_{H2O} is water content in the system) pseudosection (Fig. DR8a). Calculations showed that at $M_{H2O} > 1.5$ wt%, H_2O appears as a free fluid phase in the subsolidus resulting in decrease of the solidus (Fig. DR8a). Isopleths of X_{Ca} and

X_{Mg} in garnet and X_{Mg} in biotite are sub-parallel to the M_{H2O} axis above ~1.2 wt% H_2O (Fig. DR8b), indicating that mineral compositions are independent of the water content in this interval. The better convergence of mineral compositions of the migmatitic metapelite is observed at 1.3–1.4 wt% H_2O. Thus, 1.4 wt% H_2O has been taken for further calculation of the P-T pseudosection.

The P-T phase diagram for the high-Al migmatitic metapelite is subdivided into cordierite-free and cordierite-bearing sections (Fig. 10a, b). Cordierite appears at temperatures above 800°C and pressures below 7 kbar, so the predominant portion of the diagram is cordierite-free. Isopleths of X_{Mg}^{Grt} and X_{Mg}^{Bt} are subvertical suggesting that a decrease of pressure would not change Mg-numbers of both minerals, but dramatically change grossular content in garnet (Fig. 10b). Perchuk et al. (2008) reported rare garnets with X_{Ca} up to 0.078 at $X_{Mg} = 0.26$ from the high-Al metapelite at O6-19 (same outcrop as present study; Fig. 1d). Based on the pseudosection, it follows that such composition of garnet corresponds to pressure about 9.5 kbar at temperatures 780–790 °C (area I in Fig. 10b). Predominant type of garnet in the metapelite with $X_{Ca} = 0.03$–0.04 and X_{Mg} varying from 0.25 up to 0.32 reflect much lower-pressure conditions, below 6.0 kbar at comparable or slightly higher temperature (area II in Fig. 10b). At these conditions, cordierite coexisting with garnet and sillimanite forms in the migmatitic metapelite. This decompression-related feature is reflected in the cordierite reaction textures in the rock (e.g., Fig. 3g, h), where cordierite with fibrous inclusions of sillimanite forms around relic garnet grains. These textures are accompanied by biotite, which forms in this assemblage below 800°C. The possible additional evidence that the high-Al migmatitic metapelite initially did not contain cordierite is the absence of cordierite inclusions in garnet and the presence of biotite, sillimanite and quartz inclusions.

Thus, variations of X_{Ca} in garnet in the high-Al migmatitic metapelite reflect notable decompression by about 3 kbar (arrow in Fig. 10b). Relics of high-Ca garnet are extremely rare (Perchuk et al., 2008), suggesting that the predominant garnet with lower X_{Ca} represent relics, which were totally re-equilibrated with Crd + Sil + Bt + Qz at lower pressure. No garnet zoning corresponding to the decompression is preserved in the metapelite. However, zoning with an abrupt decrease of X_{Ca} from 0.08 to 0.03 is observed in large garnet in leucosomes associated with the high-Al migmatitic metapelites (Fig. 5b). The abrupt zoning in X_{Ca} is accompanied by gradual prograde zoning in X_{Mg} (Fig. 5b). In fact, the pseudosection (Fig. 10b) indicates that during decompression with only slight heating in the interval of 30 to 40 °C would change X_{Mg} from 0.25 to 0.33. Combination of the gradual zoning in X_{Mg} and abrupt zoning in X_{Ca} can be readily explained by higher diffusivity of Mg and Fe with respect to Ca in garnet (e.g., Spear, 1993). Thus, zoned garnets in the leucosomes were, presumably, trapped from the host metapelite in the course of decompression, suggesting peritectic entrainment (e.g., Stevens et al., 2007).

8.1.3. Verbaard granitoid (VG8)

Pseudosection for the Verbaard granitoid was calculated at the "free" O_2 (which serves as a monitor of Fe_2O_3) content 0.01 wt%. Similar to the metapelite, the T-M_{O2} (where M_{O2} is the "free" O_2 content, wt%, in the system) showed that phase relations are dependent on the O_2 content in the system only in the subsolidus being regulated by coexistence of ilmenite, rutile and biotite (Fig. DR9). In contrast, the phase relations are independent of the "free" O_2 above solidus (Fig. DR9). Isopleths of mineral compositions (illustrated by $X_{Ca} = 0.03$–0.04 and $X_{Mg} = 0.27$–0.29 isopleths in garnet in Fig. DR9) are also independent of the "free" O_2. Water content was estimated using the T-M_{H2O} pseudosection (Fig. DR10a). Calculations showed that at $M_{H2O} > 0.4$ wt%, H_2O appears as a free fluid phase in the subsolidus resulting in decrease of the solidus (Fig. DR10a). Isopleths of X_{Ca} and X_{Mg} in garnet and X_{Mg} in biotite are sub-parallel to the M_{H2O} axis above ~0.2 wt% H_2O (Fig. DR10b), indicating that mineral compositions are independent of the water content in this interval. However, isopleths of X_{An} in plagioclase 0.235–0.245
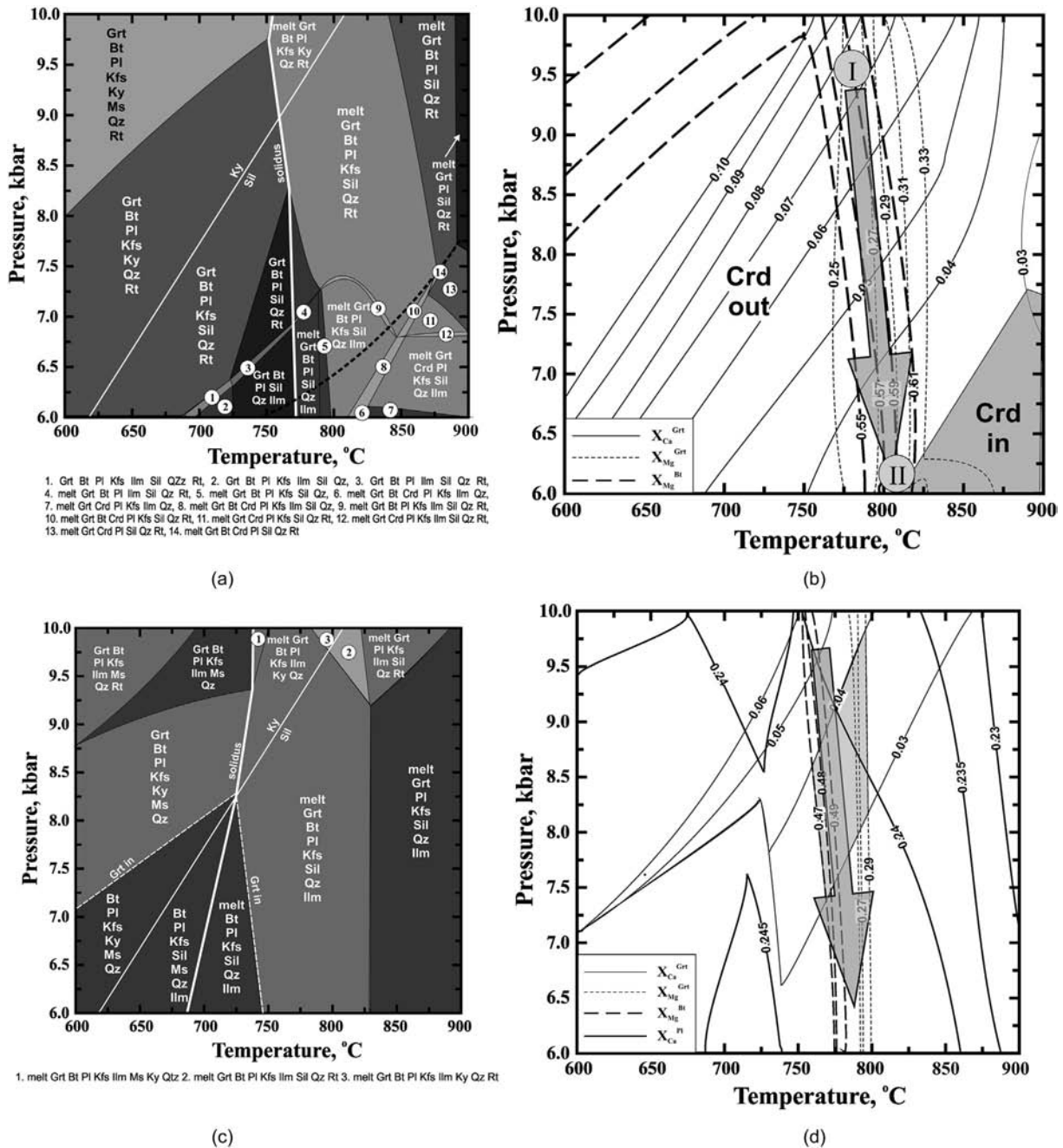
Fig. 10. (a) P-T pseudosection for the high-Al migmatitic metapelite (sample O6–19). Thick dashed line shows a limit boundary of the cordierite-bearing assemblages at H$_2$O 2 wt%. (b) Selected isopleths of X_{Ca}^{Grt}, X_{Mg}^{Grt} and X_{Mg}^{Bt} calculated for the high-Al migmatitic metapelite (sample O6–19). Grey circle (I) shows possible P-T conditions of the high-pressure stage corresponding to formation of high-Ca garnet (Perchuk et al., 2008), grey circle (II) indicates P-T conditions for beginning of cordierite formation in the course of decompression path (grey arrow). (c) P-T pseudosection for the Verbaard granitoid (sample VG8; average of samples VG8a to e in Table 1). (d) Selected isopleths of X_{Ca}^{Grt}, X_{Mg}^{Grt}, X_{Mg}^{Bt} and X_{Ca}^{Pl} calculated for the Verbaard granitoid (sample VG8). Grey field mark possible P-T conditions of the formation of the mineral assemblage in the granitoid. Grey arrow shows a probable decompression path for the Verbaard granitoid.

characteristic for the sample VG8 cross the garnet and biotite isopleths below ~0.5–0.4 wt% H$_2$O (Fig. DR10b). Thus, 0.3 wt% H$_2$O has been taken arbitrarily for further calculation of the P-T pseudosection.

Phase diagram for the composition VG8 (Fig. 10c) is subdivided into the garnet-bearing and garnet-free portions and shows a positive slope for the solidus line, which is characteristic of fluid-absent melting. The pseudosection predicts small amounts (<0.5 vol%) of sillimanite (kyanite) and muscovite reflecting peralumionous bulk composition. However, these phases can be eliminated with a slight change in bulk composition. In fact, modeling of the composition (sample TR89; see Table DR6) reported by Jaeckel et al. (1997) for the granodioritic

Verbaard granitoid, which is less peraluminous, shows no sillimanite (kyanite) and muscovite.

Pseudosection shows that at pressures above 7–8 kbar, the Verbaard granitoid contains garnet both in the subsolidus and suprasolidus (Fig. 10c). The closest convergence of the average compositional parameters $X_{Ca}^{Grt} = 0.03$–0.04, $X_{Mg}^{Grt} = 0.27$–0.29, $X_{Mg}^{Bt} = 0.47$–0.49 and $X_{Ca}^{Pl} = 0.235$–0.245, characteristic for minerals in the Verbaard granitoid, is observed in the pressure interval of 7.3 to 9.5 kbar and temperatures of 760 to 800°C within the phase field melt+Grt + Bt + Pl + Kfs + Ilm + Qz + (Sil) (Fig. 10d). At these conditions, proportions of crystalline phases are as follows (vol%): Qz ~ 32, Kfs ~16, Pl ~43, Grt ~2, Bt ~1.5–2, Ilm ~0.3,

Sil ~0.4, which is consistent with the phase proportions in the rock. The Verbaard granitoid also preserve garnets with slightly higher $X_{Ca} = 0.05$–0.055, which, according to pseudosection, indicates temperatures of 740 to 750°C at 9 to 9.5 kbar (Fig. 10d). Garnet with $X_{Ca} = 0.05$–0.06 is also present in the leucocratic veins associated with the Verbaard granitoid, although most garnets in the veins show $X_{Ca}^{Grt} = 0.03$–0.04. Together with the zoning in X_{Ca} (from 0.06 in core to 0.03 in rim) observed in garnet (Fig. 5d), the higher-Ca garnet in the veins, can be interpreted as relics trapped by the veins. Based on the isopleths (Fig. 10d), it follows that the variations of X_{Ca} of garnet from 0.06 down to 0.03 in the Verbaard granitoid and associated leucocratic veins likely reflect a decompression path from 9.0–9.5 kbar to below 7.5 kbar at probable slight heating within the interval of 740 to 800°C.

At pressures below 7–8 kbar, garnet is absent in the subsolidus of the Verbaard granitiod. A sequence of phase fields from higher temperature melt+Grt + Bt + Pl + Kfs + Qz + Ilm + (Sil) through melt+Bt + Pl + Kfs + Qz + Ilm + (Sil) to Bt + Pl + Kfs + Qz + Ilm + (Sil + Ms) in the subsolidus demonstrates that garnet leaves the granitoid assemblage via the back-reaction Grt + Kfs + melt = Bt + Pl + Qtz (e.g., Rong et al., 2017) on cooling, which follows decompression. This reaction is suggested here as a mechanism to explain the rarity of garnet in the Verbaard granitoid.

8.1.4. Comparison of the modeling results

Comparison of the results of the phase equilibria modeling for both rocks show that temperatures for formation of their garnet-bearing assemblages are similar, 760–800°C. The upper limit of pressure for the Verbaard granitoid, 9.0–9.5 kbar, is comparable with pressure for the possible stage I of evolution of the high-Al migmatitic metapelite (Fig. 10b). Both rocks were influenced by decompression, which is recorded in the decrease of grossular content in garnet at almost constant X_{Mg}. At high-pressure and low-pressure stages, 3 to 10 vol% of a granitic melt was present. During decompression, this melt likely segregated, trapping garnets including high-Ca varieties. Both granitoid and migmatitic metapelite were affected by the segregated melts. The increase of water proportion during decompression also increases the stability of cordierite in migmatitic metapelite to higher pressure and lower temperature assisting to more intense formation of this mineral as observed in the rock. This is illustrated by a dashed thick line in the pseudosection (Fig. 10a), which delineates the boundary of the cordierite-bearing region at a water content of 2 wt% in the system.

Although the composite Verbaard granitoid+leucocratic vein sample, which represents composition closer to the leucocratic vein, contains ~5 wt% K_2O (Figs. 6, 7), its composition differ from that of the melt (in wt%, SiO_2 67–68, Al_2O_3 14–15, FeO 0.6–0.7, MgO 0.16–0.17, CaO 0.4–0.5, Na_2O 3–4, K_2O 5–6, H_2O 7–8), which is predicted to coexist with the assemblage of the Verbaard granitoid at pressure 9.0–9.5 kbar and temperature 800°C. Similarly, composition of the melt (in wt%, SiO_2 66–67, Al_2O_3 14–15, FeO 0.3–0.4, MgO 0.09–0.10, CaO 0.8–0.9, Na_2O 2–3, K_2O 6–7, H_2O 9), which is predicted to be present in the migmatitic metapelite at pressure 9.0–9.5 kbar and temperature 800°C, also differs from the composition of the associated leucosome (Fig. 7a), first of all, in terms of high K_2O content and low CaO content. In order to produce the observed leucosome bulk composition, K_2O, H_2O, SiO_2 must be removed from the melt. In this case, different degree of melt loss (Brown, 2002; Nicoli et al., 2015; Sawyer, 1987; Solar and Brown, 2001; Taylor et al., 2014) could serve as a possible mechanism explaining the difference between the modeled melt composition and the present leucosome and vein compositions. The tonalitic leucosomes likely represent cumulates, which lost their interstitial evolved melt. This can happen, for instance, if crystallization was accompanied by shear-enhanced compaction (e.g., see Carvalho et al., 2016). The presence of plagioclase framework microstructures related to compaction in the leucosomes (see inset in Fig. 3o; e.g., Carvalho et al., 2016) support the inference on melt loss. On the other hand, no such microstructures are observed in the granitic leucocratic veins. Different degree of melt loss can also

explain the preservation or very slight modification of anhydrous mineral assemblages in the leucosomes and veins. An evidence for the melt loss from the leucosomes/leucocratic veins back to the metapelite/Verbaard granitoid is perthitic K-feldspar and myrmekites locally present in the rocks (Fig. 3k, t). In this scenario, the low-Al migmatitic metapelites, which differ from the high-Al one by higher contents of SiO_2 and K_2O (Fig. 6), seem to correspond to higher proportion of granitic melt and, presumably, lost less melt than the high-Al metapelite (which is thus, more residual).

8.2. Timing of event(s)

Van Reenen et al. (2008) presented U—Pb zircon ages, which indicated of two high-grade events – the earlier at 2610 ± 8 Ma and the later at 2011 ± 11 Ma – for the migmatitic metapelite that hosts garnet-bearing leucosome at O6-19 (same outcrop as in the present study; Fig. 1d). Monazites from the same sample yielded U—Pb age of 2017 ± 2 Ma (Van Reenen et al., 2008). Application of the Pb—Pb stepwise leaching (PbSL) method on garnet from the restitic domain (O6-19M) and the composite leucosome (O6-19L) from the O6-19 outcrop gave errorchron ages of 2310 ± 43 Ma and 2103 ± 820 Ma, interpreted as mixed ages that reflect the effect of the Palaeoproterozoic overprint onto the Neoarchaean Pb—Pb isotopic signature of the minerals (Boshoff, 2008). Although the nature and extent of the Paleoproterozoic overprint is less clear, the prominence of the earlier Neoarchean high-grade event on migmatitic metapelites from the Verbaard area has been pointed out by different studies (Boshoff, 2008; Perchuk et al., 2008; Van Reenen et al., 2008).

Kröner et al. (1999) reported an age of 2570 ± 4 Ma from the ~2.63 Ga Verbaard granitoid. Based on the occurrence of thin leucogranite veins that occur in the granitoid sample and which could not be removed from the sample prior to crushing, the younger age was interpreted to indicate a possible melting event related to the granitoid (cf. Kröner et al., 1999). Jaeckel et al. (1997) reported a poorly defined lower intercept age of ~1930 Ma from the ~2.65 Ga tonalitic Verbaard granitoid. Both geochronologic studies did not report any ~2 Ga overprint age from the granodioritic Verbaard granitoid. Significantly, the Neoarchean overprint age (2570 ± 4 Ma) from the Verbaard granitoid is within error similar to the age of high-grade overprint (~2.61 Ga) from the associated migmatitic metapelite from the Verbaard area. Hence the garnet-bearing anatectic leucocratic veins associated with the Vebaard granitoid is likely related to the same Neoarchean high-grade overprint event that affected the migmatitic metapelites of the Verbaard area.

8.3. Petrogenetic characterization of the Verbaard granitoid

Except for the contaminated sample, all the other Verbaard granitoid samples form a coherent group in various major, trace and REE plots (Figs. 6 to 9), and can be used for petrogenetic characterization purposes.

Prominent Neoarchean granitoid events in the Beit Bridge Complex terrane include the ~2.73–2.64 Ga Alldays biotite±amphibole-bearing granitoid (Kröner et al., 1999), ~2.68–2.62 Ga Singelele garnet-bearing leucogranite (Kröner et al., 1999; Van Reenen et al., 2008; Zeh et al., 2007), and the ~2.65–2.63 Ga Avoca (Boshoff, 2008; Van Reenen et al., 2008) and ~2.61–2.58 Ga Bulai granitoids (Laurent et al., 2014), with pyroxene-bearing and pyroxene-absent varieties. Among these granitoids, the Alldays granitoid and the Singelele leucogranite are the most voluminous, and are widely distributed within the Beit Bridge Complex. The Avoca rocks are localized as a small pluton to the northwest of Alldays area, while the Bulai granitoids constitute a composite batholith in the northern part of the Musina area. While the Alldays-Avoca-Bulai granitoids represent prominent TTG-sanukitoid magmatic episodes (Laurent et al., 2014; Rajesh et al., 2018a), the Singelele event represents

the only leucogranite magmatic event within the Beit Bridge Complex (Rajesh et al., 2018b).

Jaeckel et al. (1997), Hofmaan et al. (1998) and Kröner et al. (1999) suggested the existence of a new Neoarchean granitoid event, i.e. the ~2.65–2.62 Ga Verbaard granitoid, within the Beit Bridge Complex. According to these studies, the main reason to assume the Verbaard granitoid as a separate Neoarchean granitoid event is its different appearance in the field in the Verbaard area. As shown in the present study, the garnet-bearing leucocratic veins associated with the Verbaard granitoid are related to the Neoarchean high-grade event that affected the Verbaard area. Without the garnet-bearing leucocratic veins, it is a biotite-bearing granitoid. It could be that the so-called Verbaard granitoid is a manifestation of some other Neoarchean granitoid event in the Verbaard area. The most likely candidates are the Alldays and Avoca TTGs.

Together with the tonalitic variety dated by Jaeckel et al. (1997) (tonalitic sample in Fig. 7a), and the studied granodioritic samples, the Verbaard granitoid is comparable to the Alldays TTG which is dominated by tonalites and granodiorites (Fig. 7a). This is different from the Avoca TTG which is dominated by trondhjemites (Fig. 7a). While the Alldays TTG is metaluminous to mildly peraluminous, the Verbaard granitoid samples are mildly peraluminous (Fig. 7b). Both the Alldays TTG and Verbaard granitoid are magnesian to slightly ferroan and calcic to calc-alkalic (Fig. 7c, d). The similarity between the Alldays and Verbaard granitoids is further supported by their biotite mineral chemical compositions (Fig. 11a, b), which fall in the calc-alkaline field in the biotite discrimination diagrams of Abdel-Rahman (1994) (Fig. 11c, d).

As the composition of the source plays an important role in determining the chemistry of the melt, primary melts generated from common crustal sources may be distinguished using appropriate major-element plots (e.g., Fig. 12; Montel and Vielzeuf, 1997; Patiño Douce, 1999; Gerdes et al., 2000; Altherr and Siebel, 2002). Comparison with

experimental melts produced from a variety of source rocks indicates that Na-rich rocks like the Avoca, Alldays TTGs and Verbaard granitoid are similar to melts produced by partial melting of amphibolites (Fig. 12a, b). This is in line with the general assertion that amphibolite-derived melts are depleted in alkalis, enriched in CaO, and are commonly tonalitic-trondhjemitic-granodioritic in composition (Beard and Lofgren, 1991; Patiño Douce, 1999; Rapp et al., 1991). The contaminated Verbaard granitoid shows the effect of presence of admixed supracrustal material (Fig. 12a, b). Thus the Neoarchean biotite-bearing Verbaard granitoid (including both the tonalitic and granodioritic varieties) is an Archean TTG, with typical geochemical characteristics, generally attributed to the derivation from a metabasaltic source (e.g., Fig. 12a, b; Barker and Arth, 1976; Rapp et al., 1991; Martin, 1994; Smithies, 2000; Foley et al., 2002; Moyen, 2011). Except for the overprinting garnet-bearing leucocratic veins, the features of the Verbaard granitoid are comparable to those of the Alldays granitoid (e.g., Figs. 7, 11, 12). As shown in the present study, the overprinting garnet-bearing leucocratic veins associated with the Verbaard granitoid is a local feature, restricted to the Verbaard area and surroundings.

Moyen (2011), expanding upon the study of Halla et al. (2009) on the Archean TTG granitoids pointed out the existence of three groups of TTGs in terms of their depth of origin (translated to pressure conditions) – low-pressure TTG, medium-pressure TTG and high-pressure TTG. Using the compilation of whole-rock geochemical data given in Moyen (2011), potential trend lines associated with the low-pressure, medium-pressure and high-pressure TTGs can be delineated. The Alldays granitoid consists of two groups – an older ~2.73–2.72 Ga group similar to low-pressure TTGs and a younger ~2.65–2.64 Ga similar to medium-pressure TTGs, while the Avoca TTG is similar to high-pressure TTGs (Fig. 12c to f; see Rajesh et al., 2018a). Significantly, the studied ~2.65–2.62 Ga Verbaard granitoid samples are closely comparable to the Alldays medium-pressure TTGs (Fig. 12c to f). Thus, the
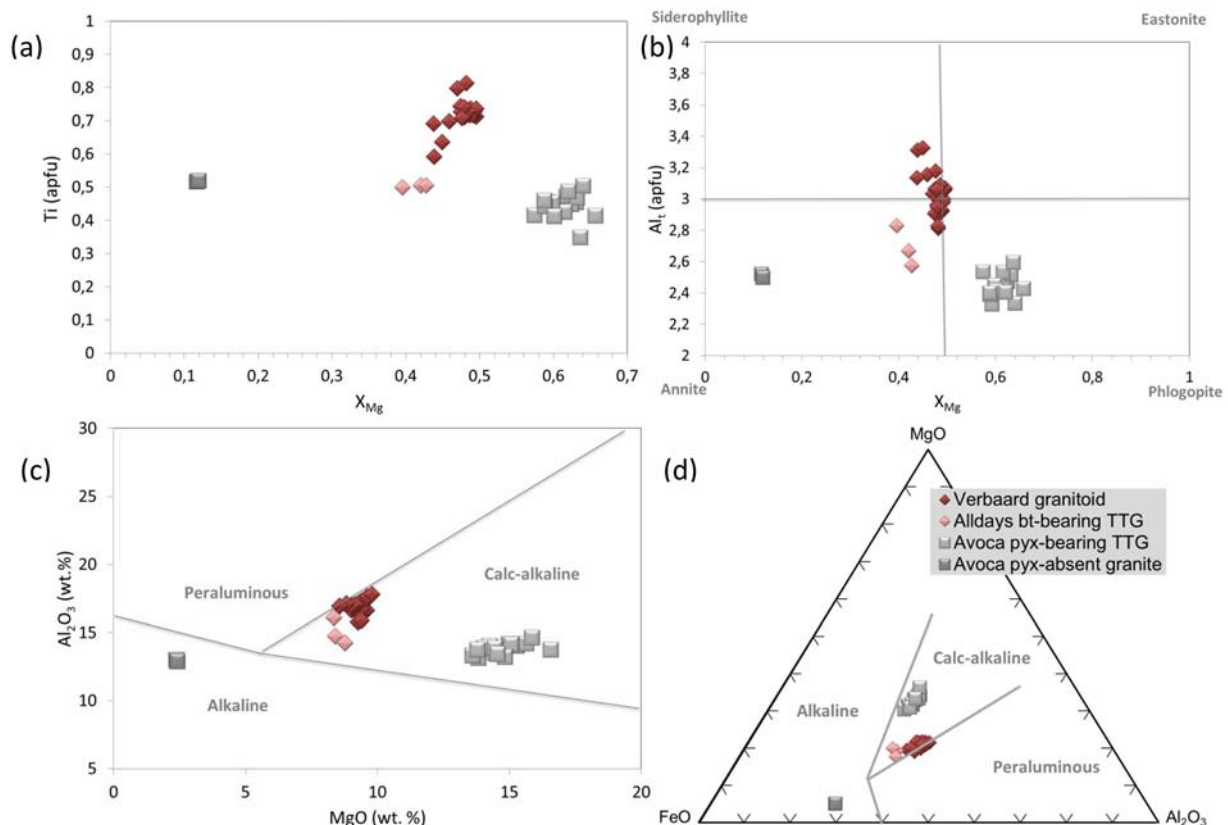

Fig. 11. Mineral chemistry based diagrams comparing the composition of biotite in the Verbaard granitoid with Alldays and Avoca granitoids from the Beit Bridge Complex terrane. The data for Alldays and Avoca granitoids is from Rajesh et al. (2018a). The fields in (c) and (d) are from Abdel-Rahman (1994).
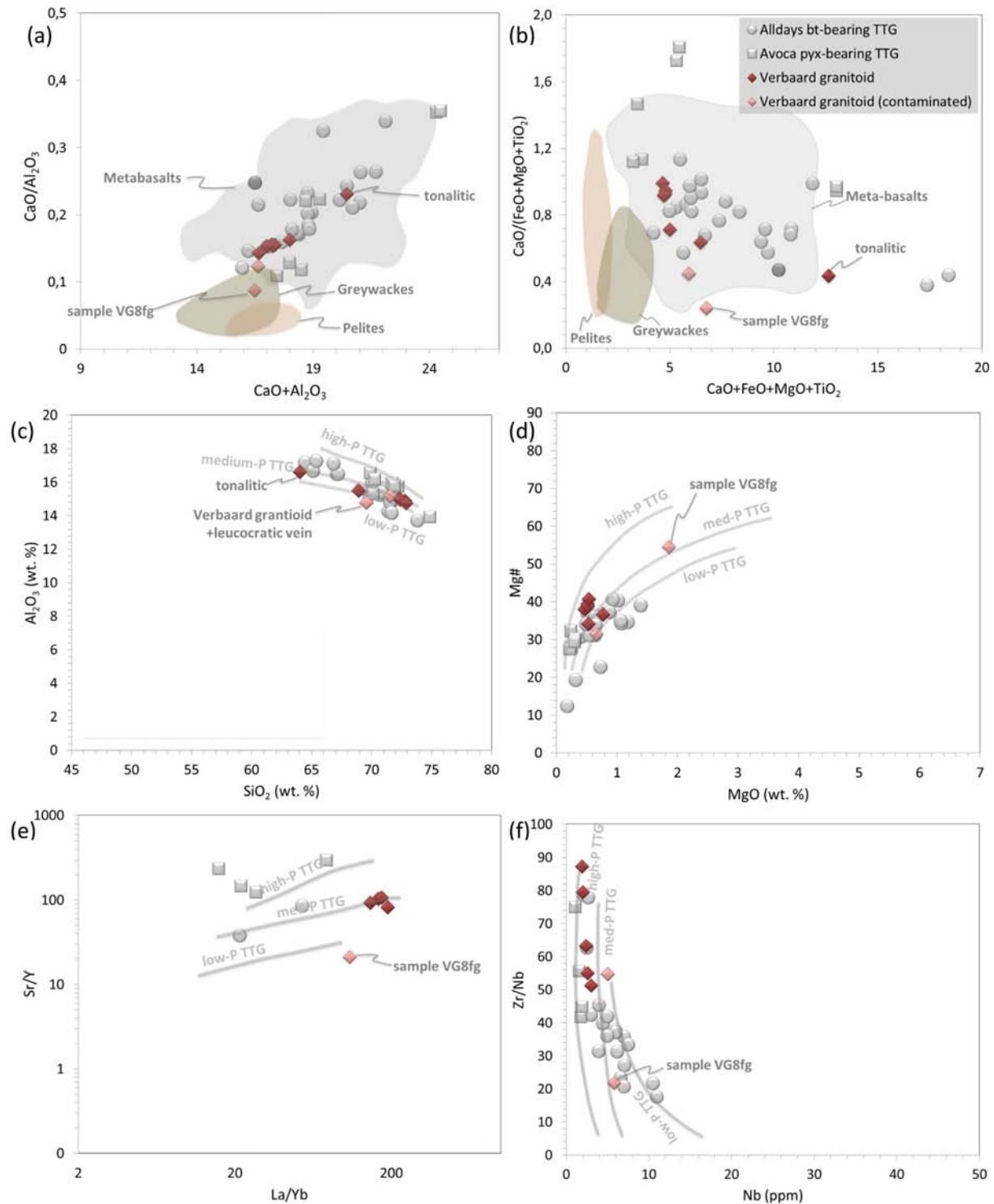
Fig. 12. (a, b) Bulk rock composition of the Verbaard granitoid compared with experimental melt compositions produced from a variety of source rocks [from Patiño Douce, 1999 and references therein]. (c to f) Representative geochemistry based diagrams comparing Verbaard granitoid with that of the different groups of Archean TTGs. Approximate trends of high-pressure, medium-pressure and low-pressure TTGs in (c to f) are drawn based on respective fields as well as compilations from Moyen (2011). Data for Alldays and Avoca granitoids are from Rajesh et al. (2018a). The tonalitic and granodioritic Verbaard granitoid samples dated by Jaeckel et al. (1997) are also included in the different plots.

Verbaard granitoid likely represents just a local manifestation of the Alldays granitoid magmatism in the specific (Verbaard) area.

9. Concluding remarks

Results of the present study are a perfect illustration for detailed evaluation of the spatial distribution of voluminous granitoids in Archean high-grade terranes. They vividly show that granitoids produced during the same magmatic cycle, but exposed in different parts of a high-grade terrane, can exhibit effects of variable local overprint events and, hence, look different.

This study presents new interpretations for the position of the Verbaard granitoids in the magmatic and metamorphic evolution of the Beit Bridge Complex terrane of the Limpopo Complex.

1. Whole-rock geochemical characteristics of the Verbaard granitoids unaffected by later overprint events (i.e. garnet- and leuocratic vein-free) are similar to Archean TTGs produced by the melting of metabasalts. Among other temporally and spatially associated Neoarchean granitoids of the Beit Bridge Complex, the closest correlatives for the Verbaard granitoids are the Alldays granitoids. Thus, the Verbaard granitoid represents just a local manifestation of the voluminous Alldays TTG granitoid magmatism in the Verbaard area.

2. The Verbaard granitoids were subjected to both metamorphic and partial melting events recorded in formation of garnet in the rocks and garnet-bearing leucocratic veins. Phase equilibria modeling indicates that rare low X_{Ca} garnets in the granitoids are re-equilibrated relics related to a low-pressure stage (7.5–6.5 kbar) of the ~2.61 Ga high-grade event that affected the rocks. In comparison, higher-Ca cores of large garnets in leucocratic veins associated with the granitoids are interpreted to represent an earlier high-pressure stage of the Neoarchean event (9.0–9.5 kbar). Thus, the veins served as potential sites for preservation of different stages of garnet formation in the granitoids. Compositional variations of garnets in the Verbaard granitoids reflect a decompression at temperatures 740 to 800 °C during the Neoarchean high-grade event.

3. Similar metamorphic evolution is recorded in garnets in country metapelites intruded by the Verbaard granitoids. Compositional evolution of garnet from the leucosomes associated with migmatitic metapelites is comparable to that of garnet in the leucocratic veins in the Verbaard granitoids, arguing for a common decompression-related evolution during the same Neoarchean high-grade event.

4. During decompression, segregated melts differently affected the Verbaard granitoids and migmatitic metapelites. The tonalitic composition of the leucosomes in metapelites shows that melt loss was prominent in them. The granitic leucocratic vein in the Verbaard granitoid represents the closest starting composition of the anatectic melt, which underwent complete crystallization without (or with negligible) melt loss.

As an extension of the results of the present study, some important strategies that could minimize misinterpretation(s) when studying overprinted Neoarchean (or Archean in general) granitoids in high-grade terranes are:

• Compare samples from non-overprinted and overprinted portions (e.g., contaminated Verbaard granitoid vs Verbaard granitoid sensu stricto) of the granitoid to understand the nature and effect of contamination. This is particularly useful when dealing with anatectic overprint, where the possible segregation of melts can complicate the compositional characteristics.

• Understand the provenance of mineral considered to have formed during the overprint event. Microprobe profiling (mineral chemical profile) of the overprint mineral from the granitoid and associated/adjacent rocks can help the provenance exercise (e.g., mineral chemical profiles of garnet from migmatitic metapelite, associated leucosome and the Verbaard granitoid).

• Evaluate the compositional (mineral chemical, whole-rock geochemical) characteristics of the overprinted granitoid with that of other granitoid events that happened before and after it (e.g., Verbaard granitoid compared to Alldays, Avoca, Singelele and Bulai granitoids).

• Carefully evaluate the spatial distribution of voluminous (widespread) granitoids, and acknowledge the possibility that the same granitoid exposed in different parts of a high-grade terrane can exhibit effects of local overprint event(s) (e.g., Alldays granitoid showing a network of garnet-bearing leucocratic veins in the Verbaard area).

Supplementary data to this article can be found online at https://doi.org/10.1016/j.lithos.2018.08.019.

References

Abdel-Rahman, A.M., 1994. Nature of biotite from alkaline, calc-alkaline and peraluminous magmas. Journal of Petrology 35, 525–541.

Aldiss, D.T., 1991. The Motloutse Complex and the Zimbabwe Craton/Limpopo Belt transition in Botswana. Precambrian Research 50, 89–109.

Altherr, R., Siebel, W., 2002. I-type plutonism in a continental back-arc setting: Miocene granitoids and monzonites from the central Aegean Sea, Greece. Contributions to Mineralogy and Petrology 143, 397–415.

Barker, F., 1979. Trondhjemite: definition, environment and hypotheses of origin. In: Barker, F. (Ed.), Trondhjemites, Dacites, and Related Rocks. Developments in Petrology. Vol. 6. Elsevier, Amsterdam, pp. 1–12.

Barker, F., Arth, J.G., 1976. Generation of trondhjemitic-tonalite liquids and Archean bimodal trondhjemite-basalt suites. Geology 4 (10), 596–600.

Beard, J.S., Lofgren, G.E., 1991. Dehydration melting and water-saturated melting of basaltic and andesitic greenstones and amphibolites at 1,3 and 6.9 kb. Journal of Petrology 32, 365–401.

Blenkinsop, T.G., 2011. Archaean magmatic granulites, diapirism, and Proterozoic reworking in the Northern Marginal Zone. In: Van Reenen, D.D., Kramers, J.D., McCourt, S., Perchuk, L.L. (Eds.), Origin and Evolution of Precambrian High-Grade Gneiss Terranes, with Special Emphasis on the Limpopo Complex of Southern Africa. Geological Society of America Memoir Vol. 207, pp. 245–268.

Boryta, M.D., Condie, K.C., 1990. Geochemistry and origin of the Archean Beit Bridge Complex, Limpopo Belt, South Africa. Journal of the Geological Society of London 147, 229–239.

Boshoff, R., 2008. The Neoarchaean to Palaeoproterozoic evolution of the polymetamorphic Central Zone of the Limpopo high-grade terrain in South Africa. [PhD thesis]. Department of Geology, the University of Johannesburg, p. 216.

Brandt, S., Klemd, R., Li, Q., Kröner, A., Brandl, G., Fischer, A., Bobek, P., Zhou, T., 2018. Pressure-temperature evolution during two granulite-facies metamorphic events (2.62 and 2.02 Ga) in rocks from the Central Zone of the Limpopo Belt, South Africa. Precambrian Research 310, 471–506.

Brown, M., 2002. Retrograde processes in migmatites and granulites revisited. Journal of Metamorphic Geology 20, 25–40.

Carvalho, B.B., Sawyer, E.W., Janasi, V.A., 2016. Crustal reworking in a shear zone: transformation of metagranite to migmatite. Journal of Metamorphic Geology 34 (3), 237–264.

Champion, D.C., Smithies, R.H., 2003. Archean granites. In: Blevin, P.L., Chappell, B.W., Jones, M. (Eds.), Magmas to Miineralisation: The Ishihara Symposium. AGSO Geoscience Australia, pp. 19–24 (Record 2003/14).

Condie, K.C., Belousova, E., Griffin, W.L., Sircombe, K.N., 2009. Granitoid events in space and time: constraints from igneous and detrital zircon age spectra. Gondwana Research 15, 228–242.

Connolly, J.A.D., 2005. Computation of phase equilibria by linear programming: A tool for geodynamic modeling and its application to subduction zone decarbonation. Earth and Planetary Science Letters 236, 524–541.

Foley, S., Tiepolo, M., Vannucci, R., 2002. Growth of early continental crust controlled by melting of amphibolites in subduction zones. Nature 417, 837–840.

Frost, B.R., Arculus, R.J., Barnes, C.G., Collins, W.J., Ellis, D.J., Frost, C.D., 2001. A geochemical classification of granitic rocks. Journal of Petrology 42, 2033–2048.

Fuhrman, M.L., Lindsley, D.H., 1988. Ternary-feldspar modeling and thermometry. American Mineralogist 73, 201–215.

Gerdes, A., Zeh, A., 2009. Zircon formation versus zircon alteration-new insights from combined U-Pb and Lu-Hf-situ LA-ICP-MS analyses, and consequences for the interpretation of Archean zircon from the Central Zone of the Limpopo Belt. Chemical Geology 261, 230–243.

Gerdes, A., Rner, G.W., Henk, A., 2000. Post-collision granite generation and HT-LP metamorphism by radiogenic heating. The Variscan South Bohemian Batholith. Journal of the Geological Society of London 157, 577–587.

Halla, J., van Hunen, J., Heilimo, E., Holtta, P., 2009. Geochemical and numerical constraints on Neoarchean plate tectonics. Precambrian Research 174, 155–162.

Halla, J., Whitehouse, M.J., Ahmad, T., Bagai, Z., 2017. Archean granitoids: an overview and significance from a tectonic perspective. Geological Society, London, Special Publication 449, 1–18.

Hofmaan, A., Kroner, A., Brandl, G., 1998. Field relationships of mid- to late Archean high-grade gneisses of igneous and sedimentary parentage in the Sand River, Central Zone of the Limpopo Belt, South Africa. South African Journal of Geology 101, 185–200.

Holland, T.J.B., Powell, R., 2011. An improved and extended internally consistent thermodynamic dataset for phases of petrological interest, involving a new equation of state for solids. Journal of Metamorphic Geology 29, 333–383.

Holzer, L., Frei, R., Barton Jr., J.M., Kramers, J.D., 1998. Unreveling the record of successive high-grade events in the Central Zone of the Limpopo Belt using Pb single phase dating of metamorphic minerals. Precambrian Research 87, 87–115.

Jaeckel, P., Kröner, A., Kamo, S.L., Brandl, G., Wendt, J.I., 1997. Late Archaean to early Proterozoic granitoidmagmatism and high-grade metamorphism in the central Limpopo Belt, South Africa. Journal of the Geological Society of London 154, 25–44.

Kemp, A.I.S., Hawkesworth, C.J., 2003. Granitic perspectives on the generation and secular evolution of the continental crust. In: Rudnick, R.L. (Ed.), The Crust. Treatise on Geochemistry. Elsevier-Pergamon, Oxford, pp. 349–410.

Kramers, J.D., McCourt, S., Roering, C., Smit, C.A., Van Reenen, D.D., 2011. Tectonic models proposed for the Limpopo Complex: Mutual compatibilities and constraints. Geological Society of America Memoir 207, 311–324.

Kröner, A., Jaechel, P., Brandl, G., Nemchin, A.A., Pidgeon, R.T., 1999. Single zircon ages for granitoids gneisses in the Central Zone of the Limpopo belt, southern Africa and geodynamic significance. Precambrian Research 93, 299–337.

Kröner, A., Brandl, G., Brandt, S., Klemd, R., Xie, H., 2018. Geochronological evidence for Archaean and Palaeoproterozoic polymetamorphism in the Central Zone of the Limpopo Belt, South Africa. Precambrian Research 310, 320–347.

Laurent, O., Martin, H., Moyen, J.F., Doucelance, R., 2014. The diversity and evolution of late-Archean granitoids: evidence for the onset of "modern-style" plate tectonics between 3.0 and 2.5 Ga. Lithos 205, 208–235.

Martin, H., 1994. The Archean gey gneisses and the genesis of the continental crust. In: Condie, K.C. (Ed.), Archean Crustal Evolution, Development in Precambrian Geology. Elsevier, Amsterdam, pp. 205–260.

Montel, J.M., Vielzeuf, D., 1997. Partial melting of metagreywackes, Part II. Compositions of minerals and melts. Contributions to Mineralogy and Petrology 128, 176–196.

Mouri, H., Whitehouse, M.J., Brandl, G., Rajesh, H.M., 2009. A magmatic age and four successive metamorphic events recorded in zircons from a single meta-anorthosite sample in the Central Zone of the Limpopo Belt, South Africa. Journal of the Geological Society of London 166, 827–830.

Moyen, J.F., 2011. The composite Archean grey gneisses: petrological significance, and evidence for a non- unique tectonic setting for Archean crustal growth. Lithos 123, 21–36.

Nicoli, G., Stevens, G., Moyen, J.-F., Frei, D., 2015. Rapid evolution from sediment to anatectic granulite in an Archean continental collision zone: the example of the Bandelierkop Formation metapelites, South Marginal Zone, Limpopo Belt, South Africa. Journal of Metamorphic Geology 33, 177–202.

O'Connor, J.T., 1965. A classification of quartz rich igneous rocks based on feldspar ratios. US Geological Survey Professional Papers 525B, 79–84.

Patiño Douce, A.E., 1999. What do experiments tell us about the relative contributions of crust and mantle to the origin of granitic magmas? In: Castro, A., Fernandez, C., Vigneresse, J.L. (Eds.), Understanding granites. Integrating New and Classical Techniques. Journal of the Geological Society, Special Publication 158, pp. 55–75

Perchuk, L.L., Van Reenen, D.D., Varlamov, D.A., Tabatabaeimanesh, Van Kal, S.M., Boshoff, R., 2008. P-T record of two high-grade metamorphic events in the Central Zone of the Limpopo Complex, South Africa. Lithos 103, 70–105.

Rajesh, H.M., Belyanin, G.A., Van Reenen, D.D., 2018a. Three tier transition of Neoarchean TTG-sanukitoid magmatism in the Beit Bridge Complex, Southern Africa. Lithos 296–299, 431–451.

Rajesh, H.M., Belyanin, G.A., Safonov, O.G., Vorster, C., Van Reenen, D.D., 2018b. Garnet-Bearing Low-Sr and High-Sr Singelele Leucogranite: A Record of Neoarchean Episodic Melting in Collisional Setting and Paleoproterozoic Overprint in the Beit Bride Complex, Southern Africa (submitted).

Rapp, R.P., Watson, E.B., Miller, C.F., 1991. Partial melting of amphibolites/eclogites and the origin of a rchean trondhjemites and tonalities. Precambrian Research 51, 1–25.

Rong, W., Zhang, S.B., Zheng, Y.F., 2017. Back-reaction of peritectic garnet as an explanation for the origin of mafic enclaves in S-type granite from the Jiuling Batholith in South China. Journal of Petrology 58 (3), 569–598.

Sawyer, E.W., 1987. The role of partial melting and fractional crystallization in determining discordant migmatite leucosome compositions. Journal of Petrology 28, 445–473.

Shand, S.J., 1943. The Eruptive Rocks. 2nd edition. John Wiley, New York, p. 444.

Smit, C.A., van Reenen, D.D., Roering, C., Boshoff, R., Perchuk, L.L., 2011. Neoarchean to Paleoproterozoic evolution of the polymetamorphic Central Zone complex. Vol. 207. The Geological Society of America Memoir, pp. 213–244.

Smithies, R.H., 2000. The Archaean tonalite–trondhjemite–granodiorite (TTG) series is not an analogue of Cenozoic adakite. Earth and Planetary Science Letters 182, 115–125.

Solar, G.S., Brown, M., 2001. Petrogenesis of migmatites in Maine, USA: possible source of peraluminous leucogranite in plutons. Journal of Petrology 42, 789–823.

Stevens, G., Villaros, A., Moyen, J.F., 2007. Selective peritectic garnet entrainment as the origin of geochemical diversity in S-type granites. Geology 35 (1), 9–12.

Sun, S.S., McDonough, W.E., 1989. Chemical and isotopic systematics of oceanic basalts: implications for mantle composition and processes. In: Saunders, A.D., Norry, M.J. (Eds.), Magmatism in the Ocean Basins: Geological Society of London, Special Publication. Vol. 42, pp. 13–345.

Taylor, J., Nicoli, G., Stevens, G., Frei, D., Moyen, J.-F., 2014. The process that control leucosome composition in metasedimentary granulites: perspectives from the Southern Marginal Zone. Limpopo Belt, South Africa. Journal of Metamorphic Geology 32, 713–742.

Van Reenen, D.D., Perchuk, L.L., Smit, C.A., Varlamov, D.A., Boshoff, R., Huizenga, J.M., Gerya, T.V., 2004. Structural and P-T evolution of a major cross fold in the Central Zone of the Limpopo high-grade terrane, South Africa. Journal of Petrology 45, 1413–1439.

Van Reenen, D.D., Boshoff, R., Smit, C.A., Perchuk, L.L., Kramers, J.D., McCourt, S.M., Amstrong, R.A., 2008. Geochronological problems in the Limpopo Complex, South Africa. Gondwana Research 14, 644–662.

Van Reenen, D.D., Smit, C.A., Perchuk, L.L., Roering, C., Boshoff, R., 2011. Thrust exhumation of the Neoarchaen ultrahigh-temperature Southern Marginal Zone, Limpopo Complex: Convergence of decompression-cooling paths in the hanging wall and prograde P-T paths in the footwall. Geological Society of America Memior 207, 189–212.

White, R.W., Powell, R., Holland, T.J.B., Worley, B.A., 2000. The effect of TiO_2 and Fe_2O_3 on metapelitic assemblages at greenschist and amphibolite facies conditions: mineral equilibria calculations in the system K_2O-FeO-MgO-Al_2O_3-SiO_2-H_2O-TiO_2-Fe_2O_3. Journal of Metamorphic Geology 18, 497–512.

White, R.W., Powell, R., Holland, T.J.B., Johnson, T.E., Green, E.C.R., 2014. New mineral activity–composition relations for thermodynamic calculations in metapelitic systems. Journal of Metamorphic Geology 32, 261–286.

Whitney, D.L., Evans, B.W., 2010. Abbreviations for names of rock-forming minerals. American Mineralogist 95, 185–187.

Zeh, A., Gerdes, A., Klemd, R., Barton Jr., J.M., 2007. Archaean to Proterozoic crustal evolution in the Central Zone of the Limpopo Belt (South Africa/Botswana): constraints from combined U–Pb and Lu–Hf isotope analyses of zircon. Journal of Petrology 48, 1605–1639.

Zeh, A., Gerdes, A., Barton Jr., J., Klemd, R., 2010. U-Th and Lu-Hf systematics of zircon from TTG's, leucosomes, meta-anorthsites and quartzites of the Limpopo Belt (South Africa): constraints for the formation, recycling and metamorphism of Palaeoarchaean crust. Precambrian Research 179, 50–68.